Progress In Electromagnetics Research C, Vol. 136, 23–36, 2023

High Isolation Compact Two Port 5G MIMO Diversity Antenna with Asymmetrical Feed and Partial Ground Structure

Sanket Nirmal[1], Sumit Kumar[1], and Richa Chandel[2, *]

Abstract—This paper presents a forthcoming compact high-performance two-element multiple-input-multiple-output (MIMO) diverse antenna for wireless-LAN 5 GHz band and sub-6 GHz 5G (NR) band. The proposed antenna consists of two symmetrical antenna elements with an inverted T-shaped ground structure. The antenna attributes such as S-parameters, realized gain, current distribution, and radiation patterns are studied. Additionally, MIMO performance is also investigated in terms of envelope correlation coefficient (ECC), diversity gain (DG), total active reflection coefficient (TARC), and multiplexing efficiency. The antenna covers the entire 5G band for wireless communication, with an effective band (−10-dB) of 2.92 to 5.72 GHz (provides bandwidth of 2.8 GHz). The obtained values indicate that the measured performance is in reasonable agreement with simulated one. Additionally, efficiency and gain were around 95% and above 3 dB across the band of interest, respectively.

1. INTRODUCTION

The 5th generation (5G) of portable communication devices is increasingly necessary to meet the demands of the growing traffic on the internet. This reason has led to the installation of cellular systems 1's within a few hundred meters, and wireless local area networks (LANs) have been installed almost everywhere to cater to this need. The devices are attractive as they have several desirable characteristics such as low delay, wide spectrum bandwidth, low power requirement in scattering environments, and they also offer high trans-reception of data in Gigabit per second (Gbps). A 5G network is said to have two primary spectrums according to ITU-R i.e., international telecommunication union radio such as millimeter wave and sub-6 GHz. Using 5G networks, mobile networks will be capable of transferring data at faster rates, while they will also be able to scale, to be connected to other networks, and be more energy-efficient.

Developing a popular smartphone and smart IoT device using 5G requires MIMO antennas. Mobile devices of the 5th generation utilize multiple-element MIMO/massive MIMO for wireless communication for base station and other applications. This occurs due to the increase in capacity gain by using more antennas on the trans-receiver. The 3rd generation partnership project (3GPP) has spectrum ranges (n77: 3.3 to 4.2) GHz, (n78: 3.3 to 3.8) GHz, (n79: 4.4 to 5) GHz [1]. Designing compact handheld gadgets in limited space becomes more challenging due to the wide range of antennas available for 5G-MIMO application. The array antenna has close profile elements restricted by close connections, and the close connection is prone to mutual coupling [2, 3]. Different decoupling techniques (mutual coupling reduction) have been examined for enhancing isolation between closely located antennas which improves MIMO performance parameters like ECC, Mean effective gain (MEG), DG, and TARC [4]. In [5], the proposed 8-element array working in dual-band (LTE 42 and 46) of size $150 \times 75\,\text{mm}^2$ with

Received 22 April 2023, Accepted 25 July 2023, Scheduled 9 August 2023

* Corresponding author: Richa Chandel (richachandel23@gmail.com).

[1] School of Electrical and Electronics Engineering, Lovely Professional University, Phagwara, Punjab, India. [2] Department of Electronics and Communication Engineering, University institute of technology, Shimla, India.

an L-type slot and a U-type monopole, and isolation of > 12 dB for 5G smartphones is discussed. The operating frequency ranges 3.4–3.6 GHz with maximum efficiency of 56% and ECC of 0.1.

In [6], the proposed MIMO structure has open ended slots of varying length ranging 2.40–2.67 GHz and 5.46–5.73 GHz with isolation 20 dB. In [7], a two elements symmetric microstrip antenna (MSA) developed on T-type ground and I-type parasitic element for good mutual coupling for sub-6 GHz application, in the same way of [8], consists of an integrated monopole low profile antenna. In [9], a dual band MIMO slot antenna with two back-to-back slots is designed to operate from 2.4 to 2.5/4.9 to 5.725 GHz. Further, in [10], a high isolation antenna with a modified H-type defected ground structure (DGS) and array decoupling structure is proposed. In [11], a parasitic element-based planer monopole is proposed with low gain and low radiation efficiency. U and T shape stubs are connected to the patch and feed line with shared ground to improve the gain, efficiency, and the mutual coupling [12].

In [13], a 2×2 antenna with fractal electro-magnetic bandgap (EBG) provides additional 4 dB better isolation with a simple structure. In [14], the proposed low-profile 8-element Inverted-F antenna (IFA) has repetitive behaviour and orthogonality resulting in complexity and poor efficiency. To achieve sufficient efficiency, the ground etching and polarization diversity are used for necessary antenna performance [15]. Further, a complementary split ring resonator (CSRR) improves isolation and correlation by pattern diversity [16]. In [17, 18], a robust microstrip antenna (MSA) with improved isolation is presented, but it is not suitable for 5G. With the use of narrow strip, the isolation enhancement is achieved with an ideal value of -22 dB used in diversified wireless communication [19]. In [20], the proposed design consists of a square shape composite right/left-handed cell, i.e., a composite right/left handed (CRLH) structure which gives the isolation ≥ 15. Additionally, the isolation value of < -25 dB in triple bands is achieved by using a hybrid dielectric resonator antenna (DRA), but it is enormous in size [21].

The MIMO antenna design is linked with many features of smartphones, base stations, and MIMO communication. As a compact antenna is today's need but in [22–25], large-size antennas are deliberated using various techniques, with moderate coupling and low-frequency coverage. In this work, our aim is to develop a MIMO antenna covering the full frequency range below 6 GHz for the fifth generation (5G) communication with a compact profile and unique performance parameters. The design and simulation are carried out on the Ansys electronic desktop (AED) HFSS 2021-R_1. It is used for optimizing the size and finding results of the antenna with a wideband operation that covers the sub-6 GHz 5G band.

In this paper, a compact high-performance two-element multiple-input-multiple-output (MIMO) diverse antenna for wireless-LAN 5 GHz band and sub-6 GHz 5G (NR) band is presented. The structure comprises two identical radiating elements with an inverted T-shaped modified ground plane as shown in Figure 1. The proposed antenna has sufficient bandwidth ranging from 2.92 to 5.72 GHz. The measured and simulated results illustrate that the proposed antenna is suitable for 5G wireless communication.

2. ANTENNA DESIGN AND CONFIGURATIONS

2.1. Antenna Design

Figure 1 depicts the geometry of the two element MIMO antenna. It comprises two identical rectangular radiating elements located on the upper surface of the substrate and a modified inverted T-shape common ground structure for isolation improvement. The overall dimension of the designed antenna is only $34\,\text{mm} \times 20\,\text{mm} = 680\,\text{mm}^2$. It is composed of a micro-structure that is fabricated on an FR-4 substrate. This substrate is composed of a material constant $(\in_r) = 4.4$, a loss tangent $(\tan\sigma)$ of 0.0025, and a thickness (t) of 1.6 mm. The two identical radiating elements consist of a square-shaped patch of length (L_p) and width (W_p) with truncated corners of length (L_1) and width $(W_2 + W_3 + W_4)$ to enhance working frequency band. Current path can be increased by reducing capacitive reactance by connecting equal stubs of the same width (W_3) and length $(L_1 + L_2)$. The coupling between ground and rectangular stubs helps to shift the frequency band towards lower side. Ground plane consists of a simple rectangular strip of length and width of $(L_g \times W)$ and an I-shape strip of width (W_{g1}) and length $(L - L_g)$ attached in the center which leads to an inverted T-shaped ground plane. The mutual coupling between the antenna elements is reduced with help of the modified ground plane. Further, to cover partial 5G bands, a U-shape slot is etched on the rectangular ground of length $(L_g - L_{g1})$ and width of (W_g). To cover all 5G-NR bands, asymmetric feed principal is used wherein, the radiating

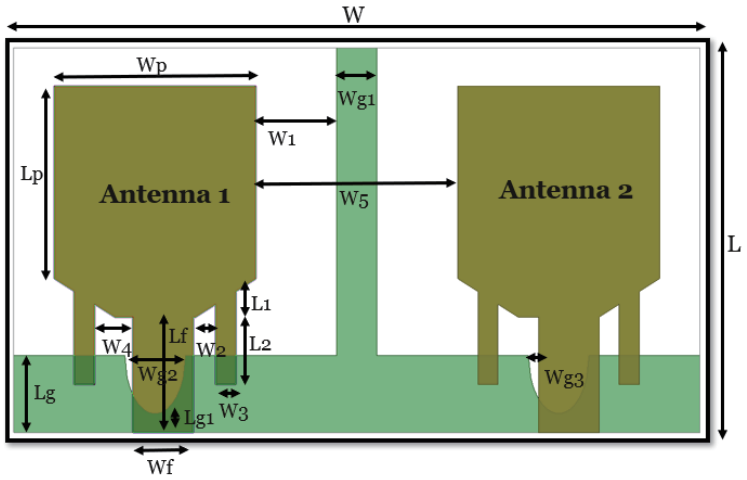

Figure 1. Configuration of 2-element MIMO with optimized parameter.

Table 1. Design parameter of the proposed antenna.

Parameters	W	L	h	L_g	W_p	L_p	W_{g1}	W_1	W_f	L_f
Unit	34	20	1.6	4	10	10	2	4	3	6
Parameters	W_{g2}	L_1	L_2	W_2	W_3	W_4	L_{g1}	W_{g3}	W_5	
Unit	3	2	3.5	1	1	2	1	0.5	10	

elements are kept aside by (W_{g3}) with reference to U-type slot. The optimized feed line of length and width $(L_f \times W_f)$ is considered to attain characteristic impedance (Zo) of 50 Ω. Table 1 shows the optimized dimension.

Figure 2 shows various design stages of the antenna transformation from a single antenna to two-element antenna arrays, and there is a noticeable improvement in bandwidth. Initially, the optimized square shape monopole fed with a microstrip-line consists of partial ground with dimensions (10×10) mm^2 with an asymmetrical feed line. In design-I, the simulated −10 dB impedance bandwidth of a rectangular patch radiator with a partial ground has a reflection coefficient (S_{11}) from 3.04–3.54 GHz.

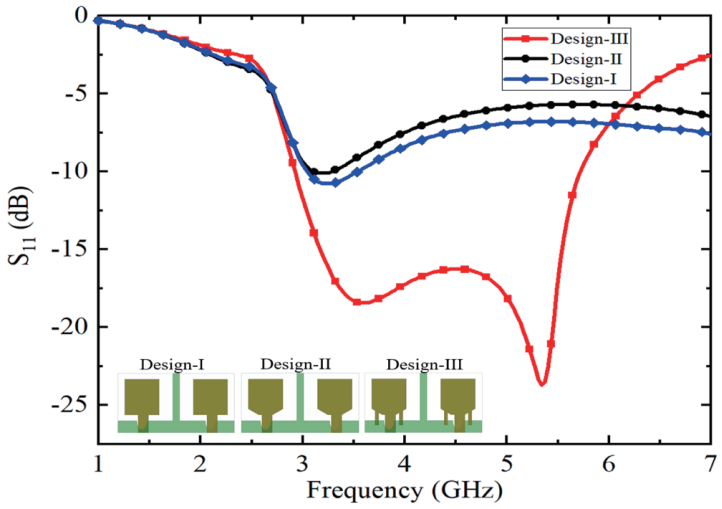

Figure 2. Simulated S_{11} against frequency for various design stages.

In design-II, the modification in a rectangular patch is introduced where the lower ends of the patch are truncated, providing a reflection coefficient (S_{11}) from 3.11–3.28 GHz. In both cases, the frequency band covered is insufficient for developing the sub-6-GHz fifth-generation (5G) antenna. Further, design-III consists of an improved antenna structure with rectangle stub lines connected at the bottom side of the patch, and partial ground improves the frequency range which occupies impedance bandwidth from 2.92 to 5.72 GHz suitable for fifth generation (5G) wireless communication.

Figure 3 depicts the effect of the width of the feedline on the S_{11} of the proposed antenna. It is observed that the change in feedline width from 1 mm to 4 mm mainly improves the impedance matching between 4.5 and 6 GHz bandwidth. Thus, the optimum value W_f is chosen as 3 mm for good impedance matching in the entire band.

Figure 4 depicts the variation in the length of the ground plane (L_g). It is observed that there is unfortunate impedance matching at 2 mm and 3 mm. Further, at 5 mm and 6 mm, a partial coverage of 5G (n77, n78, and n79) band is obtained. After optimization, for $L_g = 1$ mm, the antenna covers all 5G bands along with frequency range used for WLAN.

From Figure 5, it is notable that the width of the rectangular stub line (W_3) designated on either

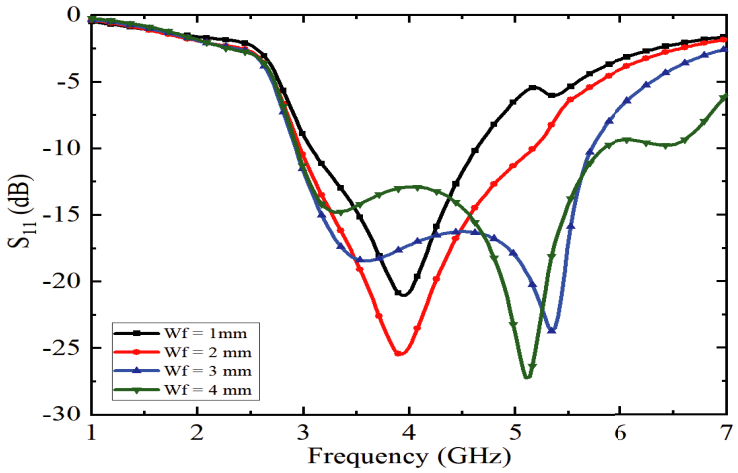

Figure 3. Simulated S-parameters against frequency for the various values of W_f. The other parameters are the same as listed in Table 1.

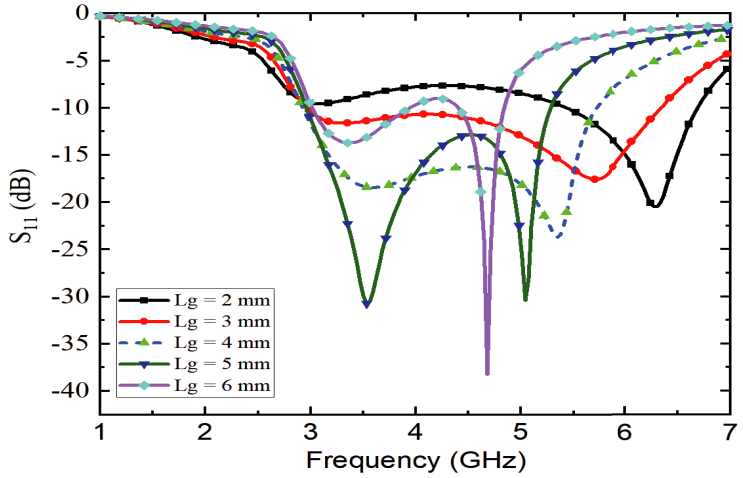

Figure 4. Simulated S-parameters against frequency for the various values of L_g. The other parameters are the same as listed in Table 1.

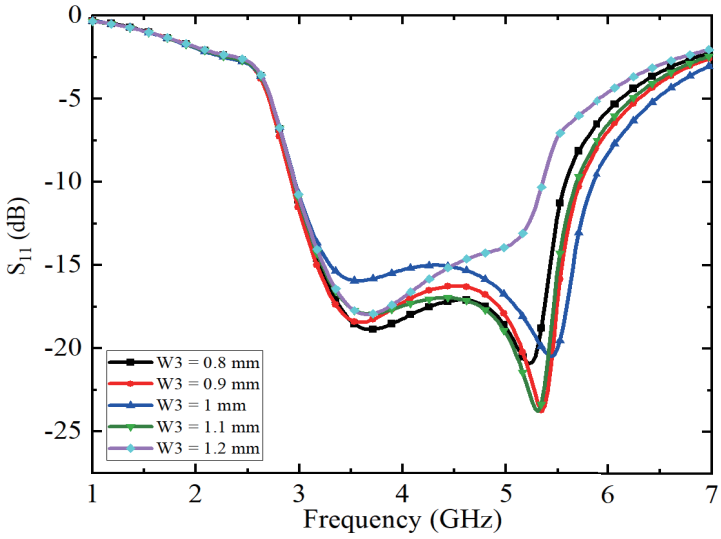

Figure 5. Simulated S-parameters against frequency for the various values of W_3. Other parameters are the same as listed in Table 1.

side of the antenna varies from 0.8 mm to 1.2 mm, which provides slight deviation in S_{11}. Thus, for $W_3 = 1$ mm, it offers appropriate matching of the impedance and covers sub-6 GHz 5G NR-new radio (n77, n78, and n79) bands. In this way, a wider bandwidth can be achieved by enhancing the ground length (L_g) and the stub-line width (W_3).

2.2. Current Distribution

To further realize the effectiveness of the antenna, the current distribution on the antenna surface is studied. The current distribution at the resonant frequency (4.5 GHz) is observed with and without I-shaped stub when port 1 is terminated with 50 Ω load, and port 2 is excited as depicted in Figure 6. The basic fundamental of this design is to minimize mutual coupling between neighbouring elements with the help of a rectangular stub connected at the bottom side of the patch so that generated field will get cancelled between adjoining patches and maintain current integrity by reducing interference using inverted T shape element, and hence direct coupling between two antennas is reduced.

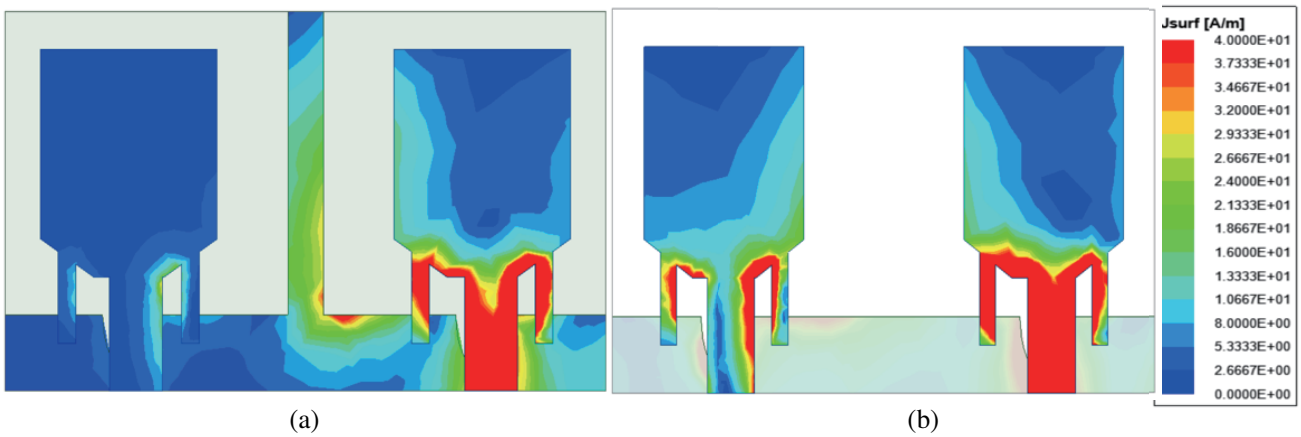

Figure 6. Current distributions of the proposed antenna with and without a I-shaped stub with port 2 (excited) at 4.5 GHz.

Further, the impedance characteristics of the antenna depend on field strength cancellation, which improves the isolation between two elements of the antenna. It is observed from Figure 6(b) that without I-shaped stub strong current is coupling between the two ports, resulting in high mutual coupling between the ports. With I-shaped stub the flow of current is concentrated on the port 2 feed line along with two rectangular stubs on both sides of radiating patch, resulting in high impedance and improved isolation as seen in Figure 6(a). Hence, the I-shaped stub in the ground plane suppresses the coupling current from port 2 to port 1.

3. EXPERIMENTAL RESULTS AND DISCUSSION

3.1. *S*-Parameters

The antenna's front patch and ground plane are constructed on a 1.6 mm thick FR-4 substrate, and using a Rohde and Schwarz ZVL series vector network analyser (VNA), antenna parameters are measured as shown in Figure 7. The measured and simulated S-parameter results are obtained as shown in Figure 8.

The simulated and measured results show an impedance bandwidth of 2.8 GHz (2.92 to 5.72 GHz) in comparison to various reported antennas shown in Table 2. The S-parameters show almost similar characteristics with little deviation in the simulated and measured values due to manufacture and soldering imperfections, including subminiature version A (SMA). Moreover, antenna elements are successfully isolated from one another, with minimum isolation value of −15 dB throughout band which satisfies 3-GPP requirement for sub-6 GHz (n77/n78/n79) communication and 5 GHz Wireless-LAN.

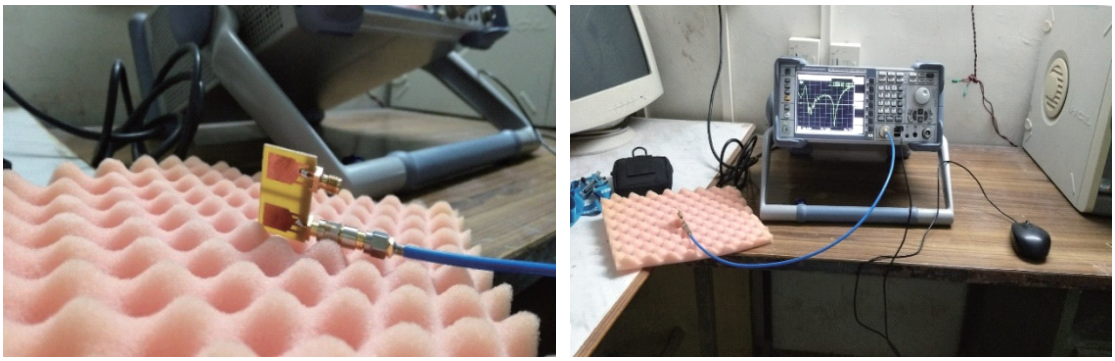

Figure 7. Measurement environment of two element MIMO using Rohde and Schwarz vector network analyser.

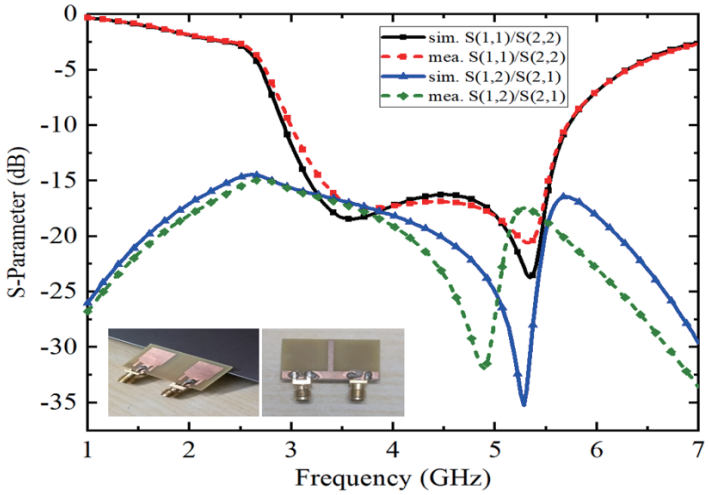

Figure 8. Simulated and measured S-parameter of proposed 5G MIMO antenna.

Table 2 shows the comparison of various MIMO antennas with the prototype antenna on the basis of size, substrate material, frequency band, isolation, ECC, and diverse MIMO types. It is observed that the proposed profile is a compact-size two-element antenna with minimum isolation, and it covers the full frequency range below 6 GHz for 5G communication.

3.2. Radiation Performance

The two-dimensional radiation pattern of proposed MIMO antenna in the E and H planes can be seen in Figure 9. During the analysis of radiation pattern. Initially, port 1 is excited, and port 2 is terminated with 50 Ω load. The E plane pattern is out of phase with each other. H plane pattern is slightly quasi-omnidirectional at low frequency, and with the high frequency, some deviation is observed

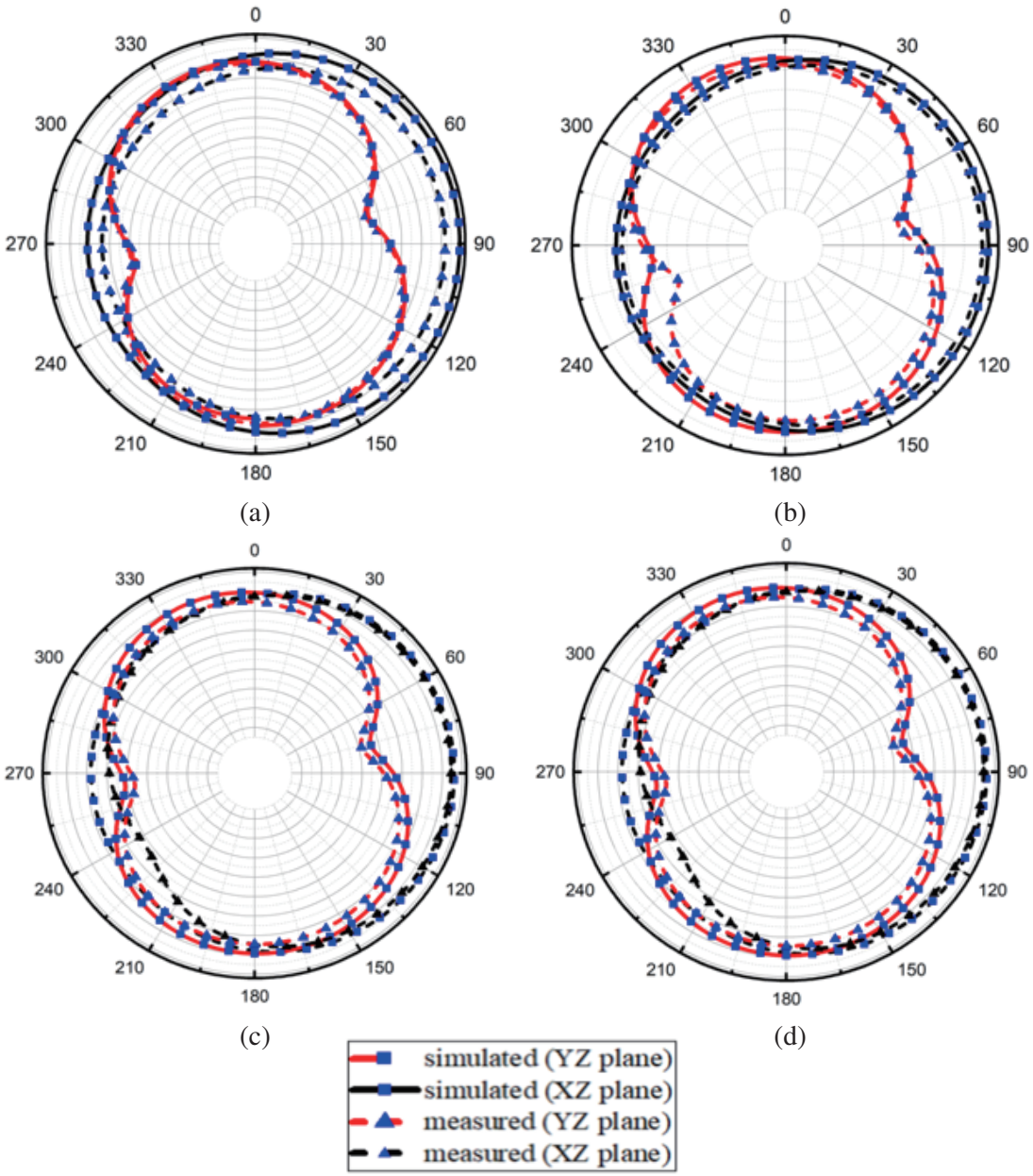

Figure 9. Measured and simulated radiation characteristics of proposed MIMO antenna. (a) 4 GHz, (b) 4.5 GHz, (c) 5 GHz, (d) 5.5 GHz.

Table 2. Comparison of proposed MIMO antenna with recently reported design.

Literature	Antenna Electrical size	Frequency band (GHz)	Isolation (dB)	Design complexity	ECC	Type
[2]	$0.35\lambda_0 \times 0.35\lambda_0$	3.2–3.9	< -20	complex	< 0.0045	Orthogonal bow-tie dipoles and U shape slot
[6]	$20.20\lambda_0 \times 0.21\lambda_0$	2.35–2.69/5.4–5.68	< -20	medium	< 0.5	Dual band slot antenna
[7]	$0.55\lambda_0 \times 0.46\lambda_0$	3.11–3.78	< -20	medium	< 0.005	Monopole parasitic element
[8]	$0.04\lambda_0 \times 0.30\lambda_0$	2.4–2.48/5.15–5.82	< -15	medium	Not given	π-shaped structure with IFA
[9]	$0.368\lambda_0 \times 0.16\lambda_0$	2.4–2.5/4.9–5.75	< -14	simple	< 0.3	Series feed with monopole slot
[10]	$0.598\lambda_0 \times 0.747\lambda_0$	3.7/4.1	< -20	medium	< 0.01	Improved ADS and H-type DGS
[12]	$0.73\lambda_0 \times 0.55\lambda_0$	5.15–5.92	< -30	medium	< 0.15	T type stub and via less structure
[13]	$0.3056\lambda_0 \times 0.76752\lambda_0$	2.43–2.50	< -24.67	simple	0.0087	fractal shaped EBG
[18]	$0.277\lambda_0 \times 0.253\lambda_0$	5.9–7.1	< -20	complex	0.005	Mushroom-type EBG with E type decoupling
[19]	$0.245\lambda_0 \times 0.396\lambda_0$	3.60–9.35	≤ -22	simple	0.084	Symmetric antennas with neutralization line
[20]	$0.2075\lambda_0 \times 0.3735\lambda_0$	2.37–2.64/3.39–3.58 /4.86–6.98	< -15	complex	0.012	Modified square loop with I-shaped slot
[21]	$0.3683\lambda_0 \times 0.5893\lambda_0$	1.5–2.55/3.21–4.0 /4.59–5.98	< -25	simple	< 0.186	Hybrid antenna with circular ring and CDRA
[22]	$1.01\lambda_0 \times 1.01\lambda_0$	1.256–1.272	< -30	medium	< 0.005	a novel decoupling slot-strip array (DSSA)
[23]	$0.312\lambda_0 \times 0.552\lambda_0$	3.7–4.2	< -21.5	medium	0.003	Hyper NL and DGS
[24]	$0.341\lambda_0 \times 0.3616\lambda_0$	3.1–5	< -22	medium	0.1	Use of NL with metal strip and circular disc.
[25]	$0.900\lambda_0 \times 0.360\lambda_0$	2.7–3.6	< -25	medium	< 0.009	Two diagonally opposite PIFA
proposed	$0.30\lambda_0 \times 0.51\lambda_0$	2.92–5.72	< -15	Simple	< 0.02	Asymmetric feed with rectangular stub lines

λ_0 is the free space wavelength.

due interaction of higher modes. Omnidirectional antennas are used in broadcast applications due to electromagnetic (EM) signal radiation/reception from any desired direction. In the radiation pattern plot, the strength of signal at various angles is observed in Figure 9, typically in the shape of doughnut. A maximum peak gain of 3.11 dB and an efficiency of 95% are achieved. The E plane pattern has attained pattern diversity and is almost bidirectional in nature, proving that there is no outside interference occurring during reception.

Figure 10 shows the realized gain and efficiency of the proposed MIMO antenna. In the entire frequency band, it is observed that the realized gain varies from 0.25 to 3.118 dB, and radiation efficiency varies between 87.19% and 95.005%.

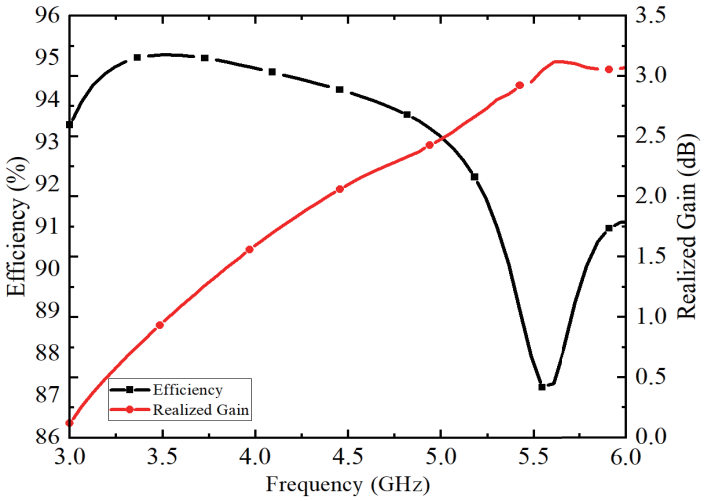

Figure 10. Realized gain and radiation efficiency of the proposed MIMO antenna.

4. MIMO PERFORMANCE

MIMO antenna behaviour is evaluated on the basis of various parameters as ECC, DG, MEG, TARC and CCL as represented in Figure 11. The ECC measures the correlation between closely spaced

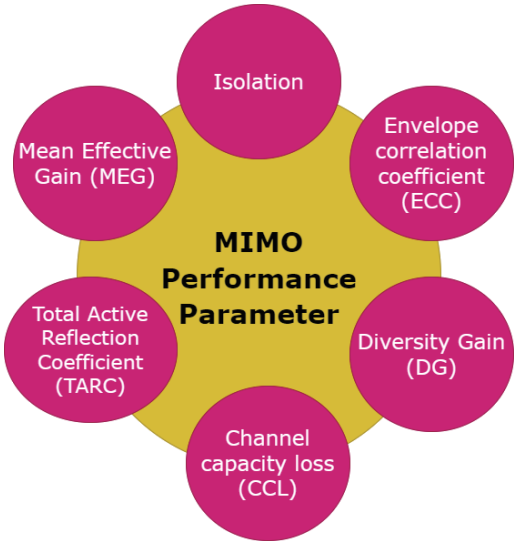

Figure 11. Various performance parameter of the MIMO antenna.

MIMO antennas, and it is calculated using scattering parameter and radiation efficiency. Coefficient of correlation is denoted by Greek letter ρ_{kl} and envelop correlation coefficient as ρ_e [6].

If $|\rho_{kl}|^2 = \rho_{ekl}$, i.e., the magnitude of square of correlation coefficient which is equal to the envelop correlation coefficient of kth and lth element therefore

$$ECC = \rho_e = \left| \frac{|S_{kk}^* S_{kl} + S_{lk}^* S_{ll}|}{\sqrt{\left(1 - |S_{kk}|^2 - |S_{lk}|^2\right)\left(1 - |S_{ll}|^2 - |S_{kl}|^2\right)\eta_{radk}\eta_{radl}}} \right|^2 \quad (1)$$

where η_{radk}, η_{radl} are the radiation efficiency, and S_{kl} is the S-parameter of the kth and lth antenna elements, respectively. Antenna coupling is an important performance parameter which gives the idea about consumption of energy in the MIMO system due to multiple antennas that are placed in closed proximity. From Equation (1), it is verified that in order to achieve sufficiently good MIMO diversity performance, we must have better isolation and correlation.

However, ideally the value of ECC should be zero, but in practical case the limit for an uncorrelated diversity antenna should be ECC < 0.5. The simulated ECC for the proposed antenna is less than 0.01, and the measured value of ECC is around 0.02 as shown in Figure 12. The diversity gain of the proposed MIMO antenna can be calculated from ECC using,

$$DG = 10\sqrt{1 - \mathrm{ECC}^2} \quad (2)$$

Diversity is calculated for $n \times n$ combination antenna, in which the data is obtained in the form of the stream from the various transmitter paths. The signal must follow a sufficient signal-to-noise ratio (SNR) value at the other end to get an improved signal strength with minimum attenuation. From Equation (2), it is concluded that the lower value of the correlation coefficient enhances the diversity gain. It is seen from Figure 12 that the simulated and measured values of the DG are almost identical and greater than 9.99 dB.

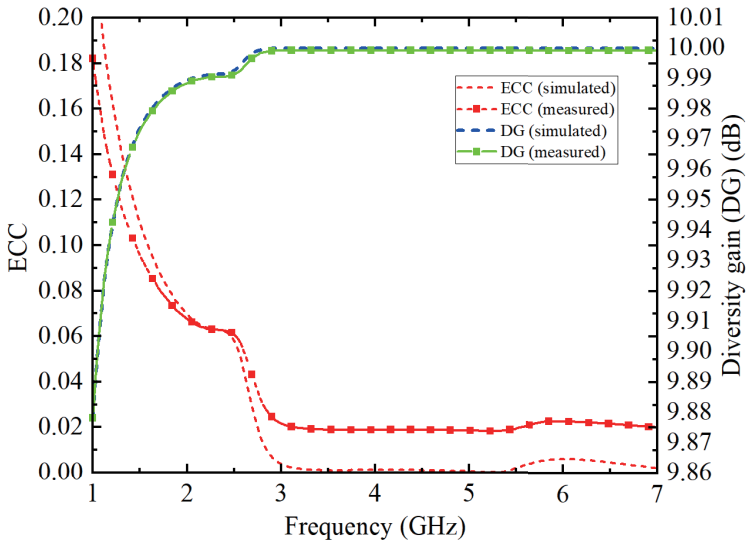

Figure 12. Simulated and measured result of ECC and DG for the proposed MIMO antenna.

It is not always enough to calculate the parameters like bandwidth and efficiency of MIMO using scattering parameters while we have multiple antennas working simultaneously, and the entire operational bandwidth is utilized by the antenna systems. Therefore, we need to use efficient methods for understanding the behaviour of antenna on the basis of performance characteristics such as TARC. The TARC is the ratio of the incident (Ii) to reflected power (Ri) in the antenna system.

If antenna has two ports, then TARC is given as,

$$T^R = \sqrt{\sum_{j=1}^{2} |R_i|^2} \Big/ \sqrt{\sum_{k=1}^{2} |I_i|^2} \tag{3}$$

$$\begin{pmatrix} R_1 \\ R_2 \end{pmatrix} = \begin{pmatrix} S_{11}S_{12} \\ S_{21}S_{22} \end{pmatrix} \begin{pmatrix} I_1 \\ I_2 \end{pmatrix} \tag{4}$$

$$\text{TARC} = \sqrt{\frac{(s_{11}+s_{12})^2 + (s_{21}+s_{22})^2}{2}} \tag{5}$$

given that Ri is a total reflected and Ii is a total incident signal at Port 1 and Port 2 of the antenna, and S-matrix for 2-element MIMO antenna is represented by S_{11}, S_{12}, S_{21}, S_{22}. Finally, R_1, R_2 and I_1, I_2 are the reflected and incident signals at port 1 and port 2, and S_{11}, S_{12}, S_{21}, and S_{22} are the reflection and transmission parameters of 2-element antenna. Figure 13 shows the graph of the simulated and measured results of the TARC. The desired value of the TARC for MIMO systems is < 0 dB. It is observed from Figure 13 that the value of TARC is less than -9 dB for the operational band.

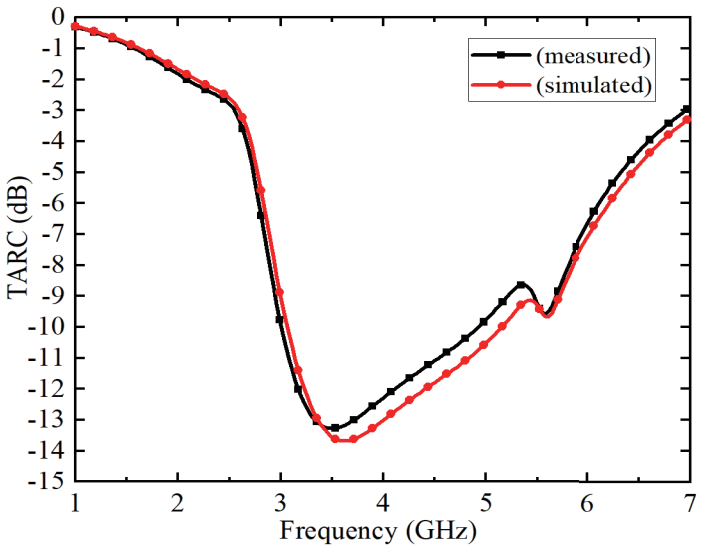

Figure 13. Simulated and measured result of the TARC for the proposed MIMO antenna.

Mean effective gain (MEG) is the ratio of mean power accepted to the average incident power with reference to an isotropic antenna, and is used to calculate gain performance in rich fading scenarios. Evaluating the effective power of each ith component of a MIMO may be done using propagated statistics and radiation patterns [25].

$$\text{MEG} = \frac{P_r}{P_i} = \int_0^{2\pi} \int_0^{\pi} \left[\frac{\text{XPR} \cdot F_\theta(\Omega) \cdot P_\theta(\Omega) + F_\phi(\Omega) \cdot P_\phi(\Omega)}{1 + XPR} \right] d\Omega \tag{6}$$

XPR stands for the cross-polarization power ratio, where Ω is the solid angle. For a uniform propagation environment, the values of XPR $= 1$ and $P_\theta = P\phi = 1/4\pi$ are taken into account. The power gain patterns of MIMO are measured w.r.t to F_θ and F_ϕ. For good MIMO performance, $\text{MEG}_j/\text{MEG}_k$ should be near unity, and the desired value of MEG varies from -3 to -4 dB as shown in Figure 14. In Table 3, the proposed two-element antenna has MEG values within specified limit, and the ratio of MEG, i.e., $\text{MEG}_1/\text{MEG}_2$, is close to unity which shows that the antenna is built with exceptional performance.

CCL is an important element while evaluating an antenna array's effectiveness in a MIMO system. In Figure 15, the proposed MIMO design is able to achieve a CCL value of less than 0.2 bits/sec/Hz,

Table 3. MEG at various frequencies of the proposed MIMO antenna.

Frequency [GHz]	MEG1	MEG1 in dB	MEG2	MEG2 in dB	MEG1/MEG2
3.0	0.49579	−3.047025314	0.498618613	−3.022315137	1.00817591
3.5	0.499583	−3.013920331	0.499262732	−3.016708509	0.999075755
4.0	0.499716	−3.012766357	0.497916021	−3.028438996	0.994824846
4.5	0.499761	−3.012378864	0.494589894	−3.057547616	0.985227131
5.0	0.499904	−3.011133019	0.488002583	−3.11577879	0.966414249
5.5	0.499416	−3.015372571	0.489728844	−3.100443158	0.972561798

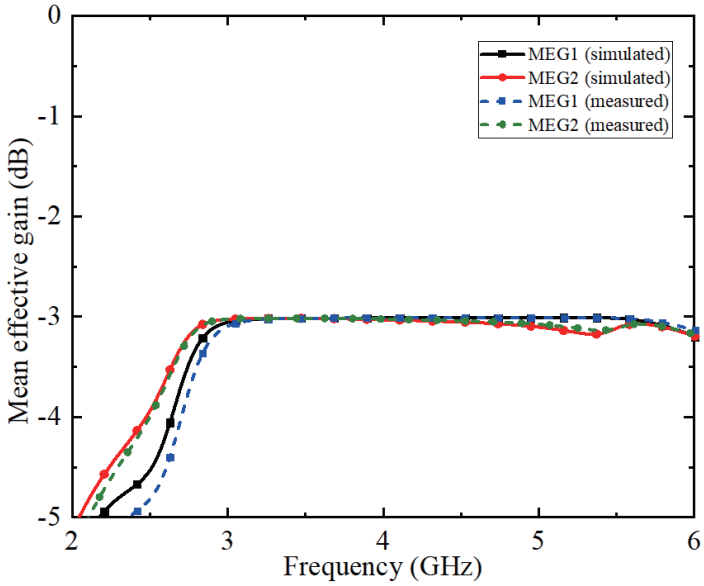

Figure 14. Simulated and measured MEG versus frequency for the proposed MIMO antenna.

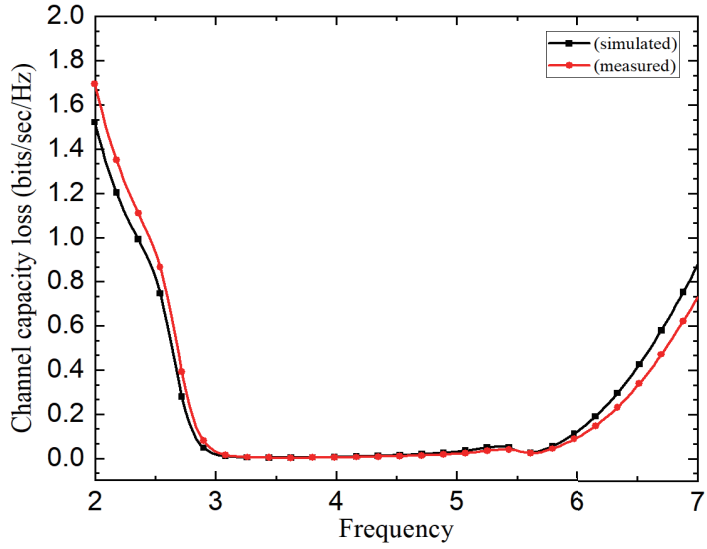

Figure 15. Simulated and measured CCL versus frequency for the proposed MIMO antenna.

which is the required value for the 5G working band, and it allows a maximum wireless throughput capability.

In a two element MIMO configuration, the correlation between antenna pair defines the impact of the 1st antenna on the 2nd antenna, which is defined mathematically [26] as,

$$C_{loss} = -\log_2 \det\left(Y^R\right) \quad \text{as,} \quad \left(Y^R\right) = \begin{bmatrix} Y_{11} & Y_{12} \\ Y_{21} & Y_{22} \end{bmatrix}. \tag{7}$$

5. CONCLUSION

An improved two-element compact MIMO antenna with close spacing and maximum impedance matching combined with a high level of isolation is presented in this paper. The results reveal that the sub-6 GHz 5G antenna has a bandwidth of 2.8 GHz ranging from 2.92 GHz to 5.72 GHz with a minimum isolation value of < -15 dB. The diverse MIMO performance parameters are calculated, and the desired values are obtained as ECC < 0.02, DG > 9.999, $\text{MEG}_1/\text{MEG}_2 \cong 0.95$, TARC $\cong 0.4$, and CCL $\cong 0.2$ bits/sec/Hz. These values are within an acceptable range for optimal MIMO performance. In a nutshell, this paper presents an efficient antenna design approach that can be used to achieve high isolation 2-element MIMO antenna for WLAN/sub-6 GHz (n77, n78, and n79) 5G application. The paper contributes to the ongoing research in antenna design and provides valuable insights into the performance parameters of MIMO antennas.

REFERENCES

1. Kumar, S., A. S. Dixit, R. R. Malekar, H. D. Raut, and L. K. Shevada, "Fifth generation antennas: A comprehensive review of design and performance enhancement techniques," *IEEE Access*, Vol. 8, 163568–163593, 2020, doi: 10.1109/ACCESS.2020.3020952.
2. Li, M., X. Chen, A. Zhang, and A. A. Kishk, "Dual-polarized broad-band base station antenna backed with dielectric cavity for 5G communications," *IEEE Antennas Wireless Propag. Lett.*, Vol. 18, No. 10, 2051–2055, Oct. 2019.
3. Zhai, G., Z. N. Chen, and X. Qing, "Mutual coupling reduction of a closely spaced four-element MIMO antenna system using discrete mushrooms," *IEEE Trans. Microw. Theory Tech.*, Vol. 64, No. 10, 3060–3067, 2016.
4. Nadeem, I. and D.-Y. Choi, "Study on mutual coupling reduction technique for MIMO antennas," *IEEE Access*, Vol. 7, 563–586, 2019, doi: 10.1109/ACCESS.2018.2885558.
5. Zou, H., Y. Li, C. Y. D. Sim, and G. Yang, "Design of 8×8 dual-band MIMO antenna array for 5G smartphone applications," *Int. J. RF Microw. Comput. Eng.*, Vol. 28, No. 9, 1–12, 2018, doi: 10.1002/mmce.21420.
6. Nandi, S. and A. Mohan, "A compact dual-band MIMO slot antenna for WLAN applications," *IEEE Antennas Wirel. Propag. Lett.*, Vol. 16, 2457–2460, Jul. 2017, doi: 10.1109/LAWP.2017.2723927.
7. Liu, Y., Z. Yang, P. Chen, J. Xiao, and Q. Ye, "Isolation enhancement of a two-monopole MIMO antenna array with various parasitic elements for sub-6 GHz applications," *Micromachines (Basel)*, Vol. 13, No. 12, Dec. 2022, doi: 10.3390/mi13122123.
8. Su, S., C. T. Lee, and Y. W. Hsiao, "Compact two-inverted-F-antenna system with highly integrated π-shaped decoupling structure," *IEEE Trans. Antennas Propag*, Vol. 67, No. 9, 618–6186, Sep. 2019, doi: 10.1109/TAP.2019.2925286.
9. Soltani, S., P. Lotfi, and R. D. Murch, "A dual-band multiport MIMO slot antenna for WLAN applications," *IEEE Antennas Wirel. Propag. Lett.*, Vol. 16, 529–532, 2017, doi: 10.1109/LAWP.2016.2587732.
10. Niu, Z., H. Zhang, Q. Chen, and T. Zhong, "Isolation enhancement in closely coupled dual-band MIMO patch antennas," *IEEE Antennas Wirel. Propag. Lett.*, Vol. 18, No. 8, 1686–1690, Aug. 2019, doi: 10.1109/LAWP.2019.2928230.

11. Xu, Z., Q. Zhang, and L. Guo, "A compact 5G decoupling MIMO antenna based on split-ring resonators," *Int. J. Antennas Propag.*, 1–10, 2019.
12. Ghannad, A. A., M. Khalily, P. Xiao, R. Tafazolli, and A. A. Kishk, "Enhanced matching and vialess decoupling of nearby patch antennas for MIMO system," *IEEE Antennas Wirel. Propag. Lett.*, Vol. 18, No. 6, 1066–1070, Jun. 2019, doi: 10.1109/LAWP.2019.2906308.
13. Sharma, K. and G. P. Pandey, "Two port compact MIMO antenna for ISM band applications," *Progress In Electromagnetics Research C*, Vol. 100, 173–185, 2020.
14. Liu, D. Q., H. J. Luo,, M. Zhang,, H. L. Wen,, B. Wang,, and J. Wang, "An extremely low-profile wideband MIMO antenna for 5G smartphones," *IEEE Transactions on Antennas and Propagation*, Vol. 67, No. 9, 5772–5780, 2019, https://doi.org/10.1109/TAP.2019.2908261.
15. Jayant, S. and G. Srivastava, "Compact 4×4 proximity coupled microstrip fed UWB stepped slot MIMO antenna having triple band rejection," *Wireless Pers Commun.*, Vol. 119, 3719–3734, 2021, https://doi.org/10.1007/s11277-021-08428-w.
16. Khalid, M., S. I. Naqvi,, N. Hussain,, M. U. Rahman,, S. S. Mirjavadi,, M. J. Khan,, and Y. Amin, "4-port MIMO antenna with defected ground structure for 5G millimeter wave applications," *Electronics (Switzerland)*, Vol. 9, No. 1, 2020, https://doi.org/10.3390/electronics9010071.
17. Yue, T. W., Z. H. Jiang, and D. H. Werner, "A compact metasurface-enabled dual-band dual-circularly polarized antenna loaded with complementary split ring resonators," *IEEE Trans. Antennas Propag.*, Vol. 67, No. 2, 794–803, Feb. 2019.
18. Saxena, G., P. Jain, and Y. K. Awasthi, "High diversity gain super-wideband single band-notch MIMO antenna for multiple wireless applications," *IET Microw., Antennas Propag.*, Vol. 14, No. 1, 109–119, Jan. 2020, doi: 10.1049/iet-map.2019.0450.
19. Tiwari, R. N., P. Singh, B. K. Kanaujia, and K. Srivastava, "Neutralization technique based two and four port high isolation MIMO antennas for UWB communication," *AEU-International Journal of Electronics and Communications*, Vol. 110, 152828, 2019, doi: 10.1016/j.aeue.2019.152828.
20. Nandi, S. and A. Mohan, "CRLH unit cell loaded triband compact MIMO antenna for WLAN/WiMAX applications," *IEEE Antennas Wirel. Propag. Lett.*, Vol. 16, 1816–1819, 2017, doi: 10.1109/LAWP.2017.2681178.
21. Sharma, A., G. Das, and R. K. Gangwar, "Design and analysis of tri-band dual-port dielectric resonator based hybrid antenna for WLAN/WiMAX applications," *IET Microwaves, Antennas and Propagation*, Vol. 12, No. 6, 986–992, May 2018, doi: 10.1049/iet-map.2017.0822.
22. Gao, D., Z. Cao, X. Quan, M. Sun, S. Fu, and P. Chen, "A low-profile decoupling slot-strip array for 2×2 microstrip antenna," *IEEE Access*, Vol. 8, 113532–113542, 2020, doi: 10.1109/ACCESS.2020.3002862.
23. Ibrahim, A. M., I. M. Ibrahim, and N. A. Shairi, "Compact MIMO slots antenna design with different bands and high isolation for 5G smartphone applications," *Baghdad Sci. J.*, Vol. 16, No. 4, 1093–1102, 2019.
24. Zhang, S. and G. F. Pedersen, "Mutual coupling reduction for UWB MIMO antennas with a wideband neutralization line," *IEEE Antennas and Wireless Propagation Letters*, Vol. 15, 166–169, 2019, https://doi.org/10.1109/LAWP.2015.2435992.
25. Chattha, H. T., "4-port 2-element MIMO antenna for 5G portable applications," *IEEE Access*, Vol. 7, 96516–96520, 2019, doi: 10.1109/ACCESS.2019.2925351.
26. Karaboikis, M. P., V. C. Papamichael, G. F. Tsachtsiris, C. F. Soras, and V. T. Makios, "Integrating compact printed antennas onto small diversity/MIMO terminals," *IEEE Trans Antennas Propag.*, Vol. 56, No. 7, 2067–2078, 2008.